RSC Advances

PAPER

View Article Online
View Journal | View Issue

Cite this: *RSC Adv.*, 2021, **11**, 27199

Study on graphene oxide as a hole extraction layer for stable organic solar cells†

Jaehoon Kim,[a] Ashis K. Sarker,[b] Yeseul Park,[a] Jeonghun Kwak,[a] Hyung-Jun Song*[c] and Changhee Lee*[a]

Received 28th March 2021
Accepted 28th June 2021

DOI: 10.1039/d1ra02452c

rsc.li/rsc-advances

The development of an efficient and stable hole extraction layer (HEL) is crucial for commercializing organic solar cells (OSCs). Although a few candidates have been widely utilized as HELs for OSCs, the most appropriate material has been lacking. A few articles have recently reported graphene oxide (GO) as a well-working HEL that offers comparable performance to conventional HELs. However, a systematic study providing comprehensive insight into the GO-based OSC behavior is lacking. This article discusses broad topics, including the material properties, device efficiency, shelf lifetime, and impedance properties. We found that GO offers excellent properties, which are identical to those of conventional HELs, while the shelf lifetime shows a significant 6-fold increase. Furthermore, we discuss the significantly reduced space-charge limited region of an aged GO-based OSC compared with a PEDOT:PSS-based device, which is revealed to be a reason for the different shelf lifetime. We believe that the results will accelerate the development of GO as an HEL for OSCs and other optoelectronic devices.

Introduction

Organic solar cells (OSCs) are one of the strongest candidates for ecofriendly renewable energy sources due to their broad applicability,[1–3] low weight,[4,5] and high efficiency under low-intensity light.[6–8] Recently, numerous studies on the high efficiency[9,10] and long stability[11–13] have also been reported. However, the small range of choices for the hole extraction layer (HEL) is a considerable obstacle in commercializing OSCs. Taking into account that HEL is a broad term that includes the hole injection layer (HIL), which is usually used in light-emitting devices (LEDs) or laser diodes (LDs), the small number of candidates is a critical issue to be resolved. Regarding this problem, several candidates have been used in various articles.

The most widely utilized HEL is poly(3,4-ethylenedioxythiophene) polystyrene sulfonate (PEDOT:PSS).[14–18] While PEDOT:PSS is a conductive polymer whose conductivity can be increased up to hundreds of S cm^{-2}, PSS is a counterion that makes the complex water soluble, stabilizing the doped PEDOT and offering a matrix for PEDOT to form an aqueous dispersion. Because of its solution processability,[14–18] wide tunability,[14–16] and easy film formation,[17,18] this polymer is usually adopted as HELs and transparent conductive electrodes. However, because of the acidic nature of PEDOT:PSS, it is also well known that PEDOT:PSS deteriorates the adjacent layers, resulting in poor device stability.[19–24] Furthermore, the unignorable absorption hurdles prevent realization of the potential efficiency of OSCs.[25,26] Transition metal oxides (TMOs) are also a good option for HELs. Nevertheless, their sophisticated working mechanism,[27–29] high sensitivity to vacuum conditions,[30,31] and difficult solution processability[32] make them hard to use as the best material, especially in conventional structures.

On the other hand, graphene oxide (GO) is assessed to be a good substitute for the discussed materials due to its bandgap tunability,[33–35] high transparency,[36–38] and dielectric nature.[39,40] Although graphene possesses good conductivity[41] and energy level[42] for interface layers, its non-bandgap property makes it hard to introduce it as a charge selective layer. However, GO offers proper energy level, bandgap, and even conductivity and is easily modified by the oxidization degree.[33–35] GO and its derivative reduced graphene oxide (rGO) have been variously reported in OSC studies as a charge selective layer[43,44] and even electrodes.[45] However, a systematic review that provides comprehensive analyses into the film characteristics, device efficiency, and shelf lifetime is lacking.

This study provides detailed methods for GO synthesis and GO-based OSCs, which showed a similar performance and an outstanding shelf lifetime compared to the reference structure. Notably, the OSC exhibited a 6-fold increase in its shelf lifetime when GO was introduced instead of PEDOT:PSS. Furthermore, GO-doped PEDOT:PSS with 1 wt% ratio showed a 24% increment in efficiency than pristine PEDOT:PSS, which implies

[a]*Department of Electrical and Computer Engineering, Seoul National University, Seoul 08826, Republic of Korea. E-mail: chlee7@snu.ac.kr*

[b]*Department of Chemistry, Mawlana Bhashani Science and Technology University, Tangail-1902, Bangladesh*

[c]*Department of Safety Engineering, Seoul National University of Science and Technology, Seoul, 01811, Republic of Korea. E-mail: hj.song@seoultech.ac.kr*

† Electronic supplementary information (ESI) available. See DOI: 10.1039/d1ra02452c

a high probability of a GO as a p-dopant. For in-depth analyses, X-ray photoelectron spectroscopy (XPS), ultraviolet photoelectron spectroscopy (UPS), space-charge limited current (SCLC) analysis, and impedance spectroscopy were conducted, and the results were in line with the device current density–voltage (J–V) characteristics. The experimental details are descripted as following.

Experimental

Fabrication of OSCs

The structure of the OSCs used in the study was ITO/HEL/poly [*N*-9′-heptadecanyl-2,7-carbazole-*alt*-5,5-(4′,7′-di-2-thienyl-2′,1′,3′-benzothiadiazole)] (PCDTBT):[6,6]-phenyl C71 butyric acid methyl ester ($PC_{70}BM$)/LiF/Al. A glass substrate with patterned indium tin oxide (ITO) was prepared after sequential washes with acetone, isopropyl alcohol (IPA), and deionized water (DI). For the HEL, PEDOT:PSS was the comparative material, while GO with various annealing conditions was the experimental material. PEDOT:PSS (CLEVIOS™ HTL Solar) was purchased from Heraeus Epurio Clevios™. On the cleaned substrate, PEDOT:PSS was spin-coated with a rotational speed of 2000 rpm for 40 s, followed by an annealing treatment of 120 °C for 10 min under vacuum conditions. The synthesis method of GO is precisely described in the following text. The GO was spin-coated on the cleaned substrate with a rotational speed of 3000 rpm for 40 s, resulting in a 5 nm thick film. The GO film was annealed at 150 °C for 1 h. The active layer solution was prepared by dissolving PCDTBT : $PC_{70}BM$ (1 : 4 by weight ratio) in 1,2-dichlorobenzene (DCB) at a total concentration of 25 mg mL^{-1} with stirring overnight in a N_2-filled glovebox. The active layer solution was then spin-coated on the respective HELs and dried for 5 min under the same inert conditions. Then, LiF (0.5 nm) and Al (100 nm) were thermally evaporated sequentially.

Synthesis of GO

GO synthesis was performed according to a former article[46] using the Hummers method.[47,48] Briefly, graphite powder (3 g) was dissolved in a mixed solution of H_2SO_4 (12 mL), $K_2S_2O_8$ (2.5 g), and P_2O_5 (2.5 g) with subsequent heating at 80 °C for 4.5 h. After the procedure, the solution was cooled to room temperature, diluted with 500 mL of deionized (DI) water, and left overnight. To remove the residual acid and salts, the precipitate was filtered and washed with DI and dried overnight. The solution was then mixed with H_2SO_4 (120 mL) at 0 °C. For the next step, $KMnO_4$ (15 g) was added dropwise while maintaining the temperate at 20 °C with continuous stirring. Similar to the former step, the solution was diluted with DI water (250 mL) while maintaining the solution temperature at 50 °C. With an additional stirring of 2 h, the solution was diluted again with DI (700 mL). Furthermore, H_2O_2 (20 mL) at a 30% concentration was added to the solution, which resulted in a bright yellow mixture with bubbling. Afterward, the precipitates were filtered and washed with HCl (1 L) at a 10% concentration, which effectively removed the metal ions. With additional washing with H_2O (1 L), the remaining acid ions were removed. The final solid material was dried and dispersed in H_2O at 0.5 wt%. After purification through dialysis, the exfoliated product was sonicated to obtain a GO-dispersed solution.

Characterization of OSCs and films

The current–voltage (J–V) characteristics of the devices were measured using a Keithley 237 source measurement unit with an AM 1.5 G solar simulator (Newport, 91160A). For device stability measurement, the devices were kept in ambient conditions without any encapsulation. The optical properties were studied through absorption spectroscopy (Beckman Coulter, US/DU 70 Series). Surface topography characterization and thickness measurement was performed using atomic force microscopy (AFM) (Park Systems, XE-100). Cole–Cole plot characterization was conducted using impedance spectroscopy (Wayne Kerr Electronics, 6500B Series). X-ray photoelectron spectroscopy (XPS) (Kratos, Inc., AXIS-HSi) and ultraviolet photoelectron spectroscopy (UPS) (Kratos, Inc., AXIS-NOVA) were used for film analysis. The thermogravimetric analysis (TGA) was measured using a measurement unit (TA Instruments, SDT Q600) under N_2 atmosphere with a ramp-up speed of 10 °C min^{-1} up to 900 °C to the maximum. The Fourier-transform infrared spectroscopy (FTIR) was measured by spectroscopy (Bruker, TENSOR27) under ambient atmosphere. The Raman spectroscopy was measured by spectroscopy (Thermo Fisher, DXR2xi) with 532 nm laser excitation.

Result and discussion

Before discussing the GO-based device characteristics, fundamental analyses were performed regarding the GO. The essential optical characteristics and a topography image are shown in Fig. 1(b–d). In Fig. 1(b), the transmittance of GO film spin-coated from a 2 mg mL^{-1} dense solution is nearly 100% at 550 nm. Considering that the most widely used PEDOT:PSS intrinsically has a severe disadvantage in terms of transmittance, GO is a great candidate for OSCs and other optoelectronic devices.[25,26] The topography image measured by AFM is in good agreement with the former articles and our expectations (Fig. 1(c)). Among several solution densities, a range of 0.5–1 mg mL^{-1} was used for the optimized condition, which led to a uniform flake distribution on the ITO substrate (Fig. 1(c) and S1(a)†). In particular, the GO film of 1 mg mL^{-1} solution showed higher coverage of flakes than that of 0.5 mg mL^{-1} solution. The thickness of the utilized GO film was 5 nm (Fig. 1(d)). In comparison, over 5 mg mL^{-1} led to severe aggregation and poor topography and surface roughness (Fig. S1(b)†).

To perform elemental analysis, XPS was conducted on the GO film (Fig. 2(a)). The low binding energy peak of the C 1s core located at 284.50 eV originates from the C–C bonding in the molecular structure of GO.[49] The peaks at 286.79 and 288.31 eV originate from C–O and C=O bonding, respectively.[49] As illustrated in Fig. 1(a), numerous C–O and C=O bonds develop from the hydroxyl group (R–OH–), epoxy group (R–O–R), carboxyl

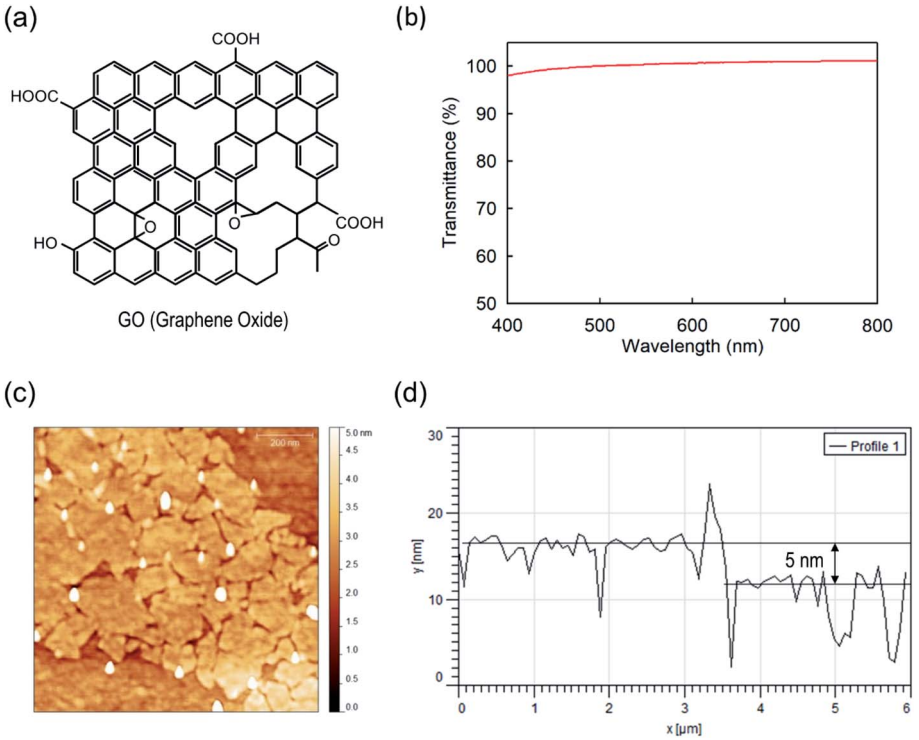

Fig. 1 (a) Schematic illustration and (b) transmittance graphene oxide (GO) film spin-coated from a 2 mg mL^{-1} dense solution. (c) Topography image of GO flakes within a GO film spin-coated from a 0.5 mg mL^{-1} dense solution, and (d) its measured thickness (~5 nm) by atomic force microscopy (AFM).

group (R–COOH). After integrating the respective peaks, it is found that the respective atomic percentages of C–C, C–O, and C=O bonds are 54.9, 39.4, and 5.7%, indicating sufficient oxidization of graphene to GO. To further validate the GO properties, the work function of the deposited GO film was measured and found to be approximately 4.6 eV (Fig. 2(b)), which is in good agreement with a former article.[50]

In the necessity of further fundamental analyses on the GO film, TGA (Fig. S2†), FTIR (Fig. S3†), and Raman spectroscopy (Fig. S4†) were conducted. In good agreement with the former GO-related TGA studies, it showed similar results upon increasing temperature. The first weight variation at 100 °C is ascribed to the removal of the moisture,[51–55] the second drop from 150 °C to 220 °C is attributed to the removal of oxygen functional groups,[51–56] and the last region above 550 °C is assigned to the removal of stable oxygen groups or combustion of remaining materials.[52–56]

Additional analyses of Fourier-transform infrared spectroscopy (FTIR) and Raman spectroscopy were conducted (Fig. S3 and S4†). In FTIR results (Fig. S3†), the GO film's absorption peaks at 1030 cm^{-1} (C–O), 1371 cm^{-1} (C–OH), 1724 cm^{-1} (C=O), and a broadband between 3000 and 3500 cm^{-1} (O–H) indicate the effective functionalization of GO.[57,58] Regarding the Raman spectroscopy result, clear D and G bands were observed (Fig. S4 and Table S1†), where D band indicates the disorder band caused by the graphite edges, and G band implies the in-phase vibration of the graphite lattice.[59] The GO (1600 cm^{-1}) showed a blue-shifted location of G band than the graphene

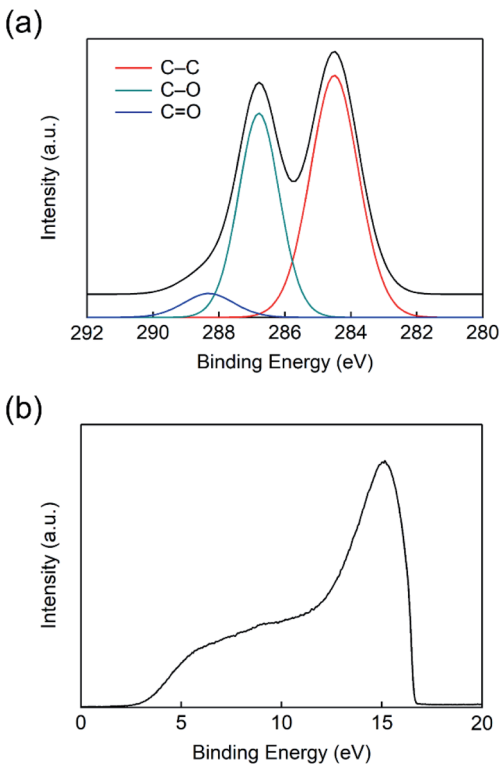

Fig. 2 (a) X-ray photoelectron spectroscopy (XPS) and (b) ultraviolet photoelectron spectroscopy (UPS) measurement result of graphene oxide (GO).

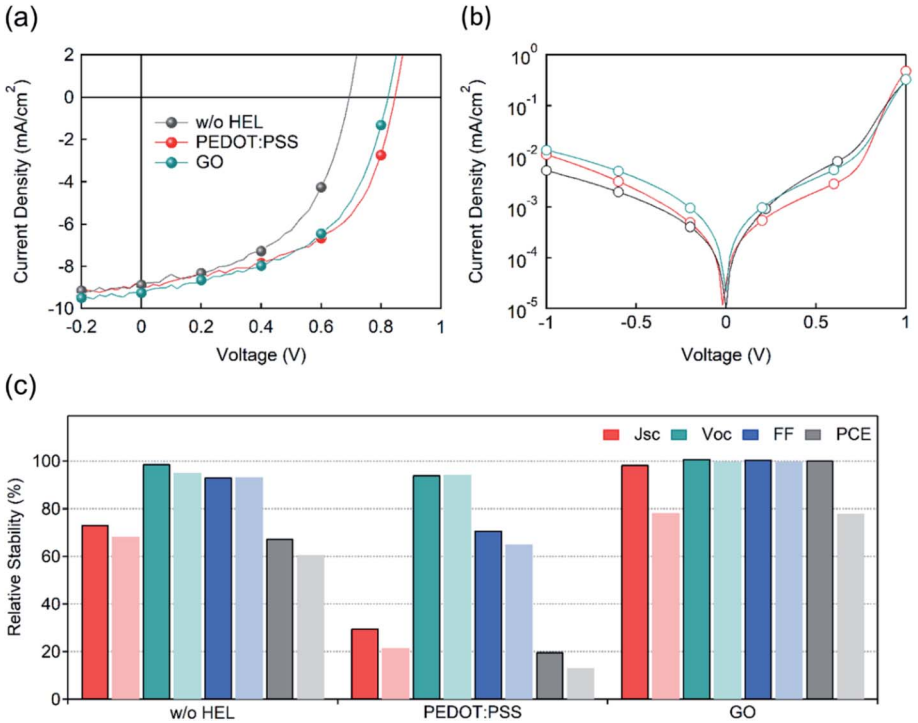

Fig. 3 (a) Current density–voltage (J–V) characteristics, (b) dark current density, and (c) normalized values of the photovoltaic parameters of devices after 2 days (solid color with border) and 4 days (pale color without border) under ambient conditions.

(1590 cm^{-1}), implying oxygenation of graphite and sp^3 carbon atoms formation.[59–61] In addition, the broadened D band of GO (FWHM = 140 cm^{-1}) than graphene (FWHM = 100 cm^{-1}) is ascribed to the reduction in sp^2 domain size by the formation of defects, vacancies, and distortions upon oxidation.[60] Furthermore, the relative peak intensity of the D band to G band (I_D/I_G) is increased from 0.985 to 1.037 when the graphene is functionalized to GO, implying the formation of oxygen-containing functional groups to the graphene plane.[60]

The J–V characteristics of OSCs with the different HELs were measured (Fig. 3(a, b) and Table 1). The photovoltaic parameters are abbreviated as follows: short-circuit current (J_{SC}), open-circuit voltage (V_{OC}), fill factor (FF), and power conversion efficiency (PCE). The performance of a device with PEDOT:PSS as an HEL showed photovoltaic parameters of J_{SC} = 9.74 mA cm^{-2}, V_{OC} = 0.85 V, FF = 0.53, and PCE = 4.36%. For accurate comparison, a device without any HEL was fabricated, and its performance was measured to be J_{SC} = 9.41 mA cm^{-2}, V_{OC} = 0.79 V, FF = 0.50, and PCE = 3.75%. Considering that the role of the HEL ranges from reducing the charge extraction barrier to accelerating the charge transport,[62] it is quite intuitive that the J_{SC} and V_{OC} of the non-HEL device showed significant decreases, leading to a 21% lower PCE. On the other hand, OSCs with optimized GO conditions showed device characteristics comparable to those with PEDOT:PSS: J_{SC} = 8.97 mA cm^{-2}, V_{OC} = 0.83 V, FF = 0.54, and PCE = 4.04%.

For further investigation, the GO was reduced with a significantly high temperature of 500 °C and applied to the device fabrication (Fig. S5†). In brief, it is reported that the GO can be effectively reduced with an extremely high temperature ranging from 300 °C to 600 °C.[63] In Fig. S5,† the OSC with reduced GO, annealed at 500 °C after GO film formation, showed inferior performance of J_{SC} = 6.34 mA cm^{-2}, V_{OC} = 0.405 V, FF = 0.369, and PCE = 0.948%. The variation is speculated to align with the former article reporting a significantly lower sheet resistance than GO,[63] resulting in a severe charge extraction imbalance within the OSC.

Most importantly, the shelf lifetime varied significantly depending on the HEL (Fig. 3(c) and S6†). It is well known that OSCs with PEDOT:PSS are very vulnerable to degradation due to

Table 1 Device characteristics for different hole extraction layer (HEL) conditions. (Average and standard deviation calculated on 6 independent devices. The numbers in parentheses are the maximum value of each condition.)

	w/o HEL	PEDOT:PSS	GO
J_{SC} (mA cm^{-2})	8.74 ± 0.55 (9.41)	8.73 ± 0.71 (9.74)	8.95 ± 0.23 (8.97)
V_{OC} (V)	0.71 ± 0.07 (0.79)	0.85 ± 0.01 (0.85)	0.81 ± 0.02 (0.83)
FF	0.50 ± 0.01 (0.50)	0.54 ± 0.01 (0.53)	0.51 ± 0.03 (0.54)
PCE (%)	3.14 ± 0.42 (3.75)	3.99 ± 0.30 (4.36)	3.71 ± 0.33 (4.04)

the acidic nature of the HEL, which deteriorates the adjacent active layer polymer and fullerene derivatives.[19–24] In line with these studies, devices with PEDOT:PSS showed unstable J_{SC} and FF, which decreased by 70% and 29%, resulting in a PCE drop of 80%, after 2 days. After 4 days of degradation, the PCE showed a total decrease of 87%. Although the device without an HEL showed relatively better stability than that with PEDOT:PSS, it still showed a PCE decrease of 40% after 4 days. On the other hand, the shelf lifetime of GO-based OSCs was measured to be much better than that under the other conditions. In particular, the GO-based device showed no decrease in PCE after 2 days, maintaining its fresh condition. After 4 days of degradation, the GO-based OSCs showed a PCE decrease of 22%. Therefore, we can conclude that GO is a great candidate for an OSC since it possesses comparable efficiency and significantly improved stability compared to PEDOT:PSS. For further confirmation, the 2 week shelf lifetime tendencies of the devices were measured (Fig. S7†), and GO-based OSC offered the most stable performance maintaining 50% of its initial value, which is a consistent result with the 4 day shelf lifetime evaluation (Fig. 3(c)).

To analyze the charge transport characteristics within the OSC, we plotted the photocurrent (J_{ph}) as a function of the effective voltage (V_{eff})[64,65] from the equation,

$$J_{ph} = q\left(\frac{9\varepsilon_0\varepsilon_r\mu}{8q}\right)^{1/4} G^{3/4} V_{eff}^{1/2} \quad (1)$$

where J_{ph} is the photocurrent, q is the elementary charge, ε_0 is the permittivity in a vacuum, ε_r is the relative permittivity, μ is the charge mobility, G is the generation rage, and V_{eff} is the effective voltage. In brief, J_{ph} is the dark current density subtracted by the current density under illumination, V_{eff} is the bias voltage (V_{bias}) deducted from the built-in voltage (V_0), where V_0 is the voltage of J_{ph} is zero. According to various former articles, the charge transport properties can be divided into ohmic, space-charge limited, and saturation regions. Concerning the J_{ph}–V_{eff} characteristics, the ohmic region shows linear dependence of J_{ph} on V_{eff}, implying an effective charge extrapolation upon light illumination. However, after some saturated point of V_{eff}, the J_{ph} starts to saturate with significantly decreased increment upon V_{eff}, considering the space-charge limited region is absent. On the other hand, J_{ph} shows a square root dependence on V_{eff}, an SCLC behavior, under the presence of space-charge limited region. In the case of OSCs, the space-charge limited region usually originates from the imbalance between electrons and holes, resulting in high recombination and a significant decrease in FF.[64,66] For the pristine OSCs (Fig. 4), all devices showed J_{ph} with a power dependence of 0.15–0.19 to V_{eff}, right after the ohmic region. However, after 4 day aging in an ambient condition without encapsulation, the devices showed different behavior depending on the HELs. While none HEL and GO-based devices showed a slight increase in the slope from 0.15 and 0.17 to 0.23 and 0.21, PEDOT:PSS-based device showed a drastic increment from 0.19 to 0.48 after the region of $V_{eff} = 0.11$ V, which is close to the square root dependence of space-charge limited conditions. Therefore, it can be interpreted that the charge transfer nature of PEDOT:PSS-based OSC changed from saturation region to SCLC region, revealing the charge asymmetry after degradation. Likewise, the FF of PEDOT:PSS device retained only 65% after 2 day degradation. This difference can be ascribed to the unfavorable acidic nature of PEDOT:PSS that is known to be detrimental to the adjacent organic layers.[19–24] However, the GO-based OSC showed an ignorable change, which is in line with the robust device characteristics upon aging, retaining 100% of its initial FF. Thus, it can be concluded that the different degree of space-charge limited behavior after degradation is the reason for the variant shelf lifetime of OSCs.

To obtain further insight, impedance spectroscopy was performed on the devices with different HELs (Fig. 5). The electrical impedance spectroscopy-derived Cole–Cole plots have been widely used in solar cell research since they provide a compelling clue for determining the resistive characteristics. The Cole–

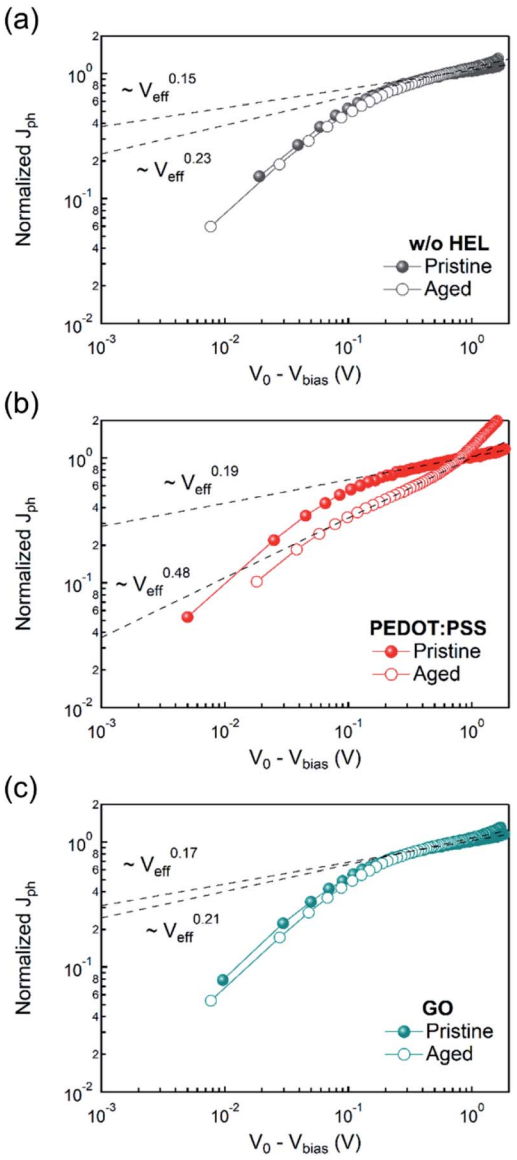

Fig. 4 Photocurrent (J_{ph}) as a function of effective voltage ($V_{eff} = V_0 - V_{bias}$) of the devices (a) without HEL, with (b) PEDOT:PSS, and (c) GO.

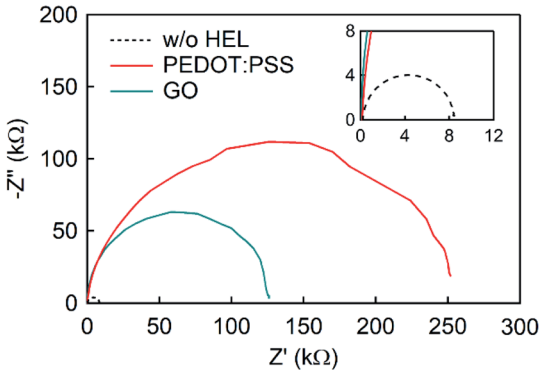

Fig. 5 Cole–Cole plot measurement by impedance spectroscopy of devices with different HELs (inset: Cole–Cole plot of device without HEL).

Cole plots are widely used to extrapolate the recombination resistance (R_{rec}) through the low-frequency arc.[67–72] While some of the studies related the decrease in R_{rec} to the enhanced charge transport,[69,72] some of the articles reversely related the increase in R_{rec} to the reduced disadvantageous charge recombination at the interface[70] or binary photoactive layer structure.[68] Assuming the equivalent circuit as a series component of each component consisting of parallel resistance and capacitance units, Cole–Cole plots were measured, varying the frequency from 100 Hz to 50 MHz. Regardless of the HEL, they showed values of approximately 150 Ω at high frequencies, attributed to the same ITO series resistance. However, they differed significantly in the low-frequency resistance, R_{rec}. At low frequency, the non-HEL device showed the lowest resistance of 8.4 kΩ, while the plot with GO showed 126 kΩ at 100 Hz, and that with PEDOT:PSS showed 252 kΩ. First, the different resistances between the non-HEL and GO devices might originate from the GO layer effectively functioning as a dielectric layer.[39,40] In addition, despite the small thickness of the GO layer of 5 nm (Fig. 1(d)), GO works well as a dielectric layer between the ITO and active layers and inhibits excessive charge migration or unfavorable charge quenching at the interface,[43] which results in an increase in R_{rec} from 8.4 kΩ to 126 kΩ. Furthermore, the GO resistive component is smaller than the PEDOT:PSS resistive component because of the significantly tiny thickness of GO despite the high conductivity of PEDOT:PSS.

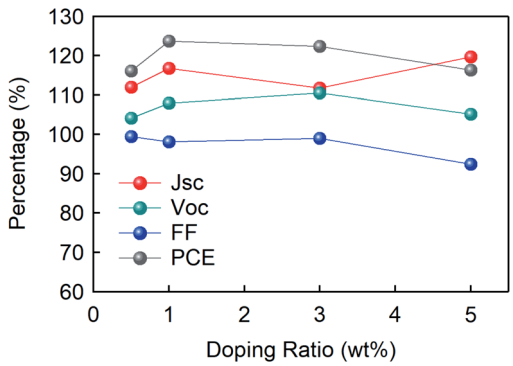

Fig. 6 Normalized values of the photovoltaic parameters of devices with composite HIL as a function of the GO doping ratio from 0.5 wt% to 3 wt% compared to pristine PEDOT:PSS.

It is also crucial that the GO works well as a p-dopant into the PEDOT:PSS, which increases device performance. In Fig. 6, the photovoltaic parameters are plotted for the GO doping ratio ranging from 0.5 wt% to 5 wt%. According to a former article, mixing GO and PEDOT:PSS efficiently enhances the device characteristics by weakening the interaction between PEDOT and PSS, and forming an extra conductive network.[73] In line with the studies, the mixed HEL showed an increased performance until some point. While J_{SC} showed a steady increase, VOC showed the highest growth in 3 wt%, while FF decreased continuously. The combined index of all other 3 factors, the PCE, showed the optimized point at 1 wt% showing 24% improvement. However, for doping ratio exceeding 25 wt% to 75 wt%, the overall device performance showed a severe decrease (Fig. S8†), which is in line with the former articles reporting disadvantageous morphology variation upon excessive composite ratio.[74] Therefore, if the stability is not a big concern, introducing the GO into the PEDOT:PSS with an optimized ratio will provide a proper method in increasing the efficiency of conventional optoelectronic devices.

Conclusions

In conclusion, we revealed that GO is one of the most appropriate candidates for HELs in OSCs. The topography images showed good surface properties without any aggregation of flakes and superior optical characteristics with high transmittance (Fig. 1). Furthermore, the initial performance of devices with GO and PEDOT:PSS showed almost comparable values (Fig. 3(a)), while they showed a massive difference in the shelf lifetime or stability in which the GO-based device exhibited a 6-fold increment compared to the PEDOT:PSS-based device (Fig. 3(c) and S6†). The enhanced shelf lifetime originated from the different degrees of involvement of space-charge limited region depending on the HELs (Fig. 4), which was supported by the following impedance spectroscopy (Fig. 5). Moreover, the mixed HEL with PEDOT:PSS and GO also offers increased efficiency, where the doping ratio of 5 wt% was found to be the optimized point with 24% improvement in PCE (Fig. 6). This study will provide practical and considerable insight into developing high-performing and substitutional HEL materials highly required in various optoelectronic areas.

Author contributions

Jaehoon Kim: conceptualization, methodology, investigation, validation, writing – original draft. Ashis Kumar Sarker: conceptualization, methodology. Yeseul Park: formal analysis. Jeonghun Kwak: resources, writing – review & editing. Hyung-Jun Song: resources, supervision, validation, writing – review & editing. Changhee Lee: resources, supervision.

Conflicts of interest

There are no conflicts to declare.

Acknowledgements

This study was supported by the Research Program funded by the SeoulTech (Seoul National University of Science and Technology).

Notes and references

1 B. Lee, L. Lahann, Y. Li and S. R. Forrest, *Sustainable Energy Fuels*, 2020, **4**, 5765–5772.
2 N. C. Nicolaidis, P. V. Hollott, B. Stanwell, I. A. Gill, J. E. Bull, S. Bentsen, J. Iredale, T. M. Pappenfus, P. C. Dastoor, K. Feron, M. J. Griffith and N. P. Holmes, *J. Chem. Educ.*, 2020, **97**, 3751–3757.
3 S. Zhang, D. Tsonev, S. Videv, S. Ghosh, G. A. Turnbull, I. D. W. Samuel and H. Haas, *Optica*, 2015, **2**, 607–610.
4 M. Kaltenbrunner, M. S. White, E. D. Głowacki, T. Sekitani, T. Someya, N. S. Sariciftci and S. Bauer, *Nat. Commun.*, 2012, **3**, 770.
5 Y. Liu, N. Qi, T. Song, M. Jia, Z. Xia, Z. Yuan, W. Yuan, K.-Q. Zhang and B. Sun, *ACS Appl. Mater. Interfaces*, 2014, **6**, 20670–20675.
6 J. Luke, L. Corrêa, J. Rodrigues, J. Martins, M. Daboczi, D. Bagnis and J.-S. Kim, *Adv. Energy Mater.*, 2021, **11**, 2003405.
7 R. Steim, T. Ameri, P. Schilinsky, C. Waldauf, G. Dennler, M. Scharber and C. J. Brabec, *Sol. Energy Mater. Sol. Cells*, 2011, **95**, 3256–3261.
8 P. Vincent, S.-C. Shin, J. S. Goo, Y.-J. You, B. Cho, S. Lee, D.-W. Lee, S. R. Kwon, K.-B. Chung, J.-J. Lee, J.-H. Bae, J. W. Shim and H. Kim, *Dyes Pigm.*, 2018, **159**, 306–313.
9 Y. Wei, J. Yu, L. Qin, H. Chen, X. Wu, Z. Wei, X. Zhang, Z. Xiao, L. Ding, F. Gao and H. Huang, *Energy Environ. Sci.*, 2021, **14**, 2314–2321.
10 L. Zhu, M. Zhang, G. Zhou, T. Hao, J. Xu, J. Wang, C. Qiu, N. Prine, J. Ali, W. Feng, X. Gu, Z. Ma, Z. Tang, H. Zhu, L. Ying, Y. Zhang and F. Liu, *Adv. Energy Mater.*, 2020, **10**, 1904234.
11 W. Yang, Z. Luo, R. Sun, J. Guo, T. Wang, Y. Wu, W. Wang, J. Guo, Q. Wu, M. Shi, H. Li, C. Yang and J. Min, *Nat. Commun.*, 2020, **11**, 1218.
12 L. Duan and A. Uddin, *Adv. Sci.*, 2020, **7**, 1903259.
13 L.-Y. Su, H.-H. Huang, Y.-C. Lin, G.-L. Chen, W.-C. Chen, W. Chen, L. Wang and C.-C. Chueh, *Adv. Funct. Mater.*, 2021, **31**, 2005753.
14 F. J. Lim, K. Ananthanarayanan, J. Luther and G. W. Ho, *J. Mater. Chem.*, 2012, **22**, 25057–25064.
15 J. P. Thomas, L. Zhao, D. McGillivray and K. T. Leung, *J. Mater. Chem. A*, 2014, **2**, 2383–2389.
16 B. Kadem, W. Cranton and A. Hassan, *Org. Electron.*, 2015, **24**, 73–79.
17 G.-E. Kim, D.-K. Shin, J.-Y. Lee and J. Park, *Org. Electron.*, 2019, **66**, 116–125.
18 G. Kim, J. Lee, D. Shin and J. Park, *IEEE Trans. Electron Devices*, 2019, **66**, 1041–1049.
19 J. Cameron and P. J. Skabara, *Mater. Horiz.*, 2020, **7**, 1759–1772.
20 B. Y. Kadem, M. Al-Hashimi, A. S. Hasan, R. G. Kadhim, Y. Rahaq and A. K. Hassan, *J. Mater. Sci.: Mater. Electron.*, 2018, **29**, 19287–19295.
21 J. J. Lee, S. H. Lee, F. S. Kim, H. H. Choi and J. H. Kim, *Org. Electron.*, 2015, **26**, 191–199.
22 M. Kim, M. Yi, W. Jang, J. K. Kim and D. H. Wang, *Polymers*, 2020, **12**, 129.
23 H. Kim, S. Nam, H. Lee, S. Woo, C.-S. Ha, M. Ree and Y. Kim, *J. Phys. Chem. C*, 2011, **115**, 13502–13510.
24 E. Voroshazi, B. Verreet, A. Buri, R. Müller, D. Di Nuzzo and P. Heremans, *Org. Electron.*, 2011, **12**, 736–744.
25 N. Yaacobi-Gross, N. D. Treat, P. Pattanasattayavong, H. Faber, A. K. Perumal, N. Stingelin, D. D. C. Bradley, P. N. Stavrinou, M. Heeney and T. D. Anthopoulos, *Adv. Energy Mater.*, 2015, **5**, 1401529.
26 Z. Tang, A. Elfwing, J. Bergqvist, W. Tress and O. Inganäs, *Adv. Energy Mater.*, 2013, **3**, 1606–1613.
27 J. Meyer, S. Hamwi, M. Kröger, W. Kowalsky, T. Riedl and A. Kahn, *Adv. Mater.*, 2012, **24**, 5408–5427.
28 J. Meyer, M. Kröger, S. Hamwi, F. Gnam, T. Riedl, W. Kowalsky and A. Kahn, *Appl. Phys. Lett.*, 2010, **96**, 193302.
29 S. Hamwi, J. Meyer, M. Kröger, T. Winkler, M. Witte, T. Riedl, A. Kahn and W. Kowalsky, *Adv. Funct. Mater.*, 2010, **20**, 1762–1766.
30 C. H. Cheung, W. J. Song and S. K. So, *Org. Electron.*, 2010, **11**, 89–94.
31 M. T. Greiner, L. Chai, M. G. Helander, W.-M. Tang and Z.-H. Lu, *Adv. Funct. Mater.*, 2012, **22**, 4557–4568.
32 J.-H. Huang, T.-Y. Huang, H.-Y. Wei, K.-C. Ho and C.-W. Chu, *RSC Adv.*, 2012, **2**, 7487–7491.
33 H. Chang, Z. Sun, Q. Yuan, F. Ding, X. Tao, F. Yan and Z. Zheng, *Adv. Mater.*, 2010, **22**, 4872–4876.
34 U. A. Méndez-Romero, S. A. Pérez-García, X. Xu, E. Wang and L. Licea-Jiménez, *Carbon*, 2019, **146**, 491–502.
35 Y. Shen, S. Yang, P. Zhou, Q. Sun, P. Wang, L. Wan, J. Li, L. Chen, X. Wang, S. Ding and D. W. Zhang, *Carbon*, 2013, **62**, 157–164.
36 G. Eda, G. Fanchini and M. Chhowalla, *Nat. Nanotechnol.*, 2008, **3**, 270–274.
37 H. A. Becerril, J. Mao, Z. Liu, R. M. Stoltenberg, Z. Bao and Y. Chen, *ACS Nano*, 2008, **2**, 463–470.
38 L. F. Lima, C. F. Matos, L. C. Gonçalves, R. V. Salvatierra, C. E. Cava, A. J. G. Zarbin and L. S. Roman, *J. Phys. D: Appl. Phys.*, 2016, **49**, 105106.
39 H. Liu, P. Xu, H. Yao, W. Chen, J. Zhao, C. Kang, Z. Bian, L. Gao and H. Guo, *Appl. Surf. Sci.*, 2017, **420**, 390–398.
40 D. Arthisree and G. M. Joshi, *Mater. Res. Express*, 2018, **5**, 075304.
41 W. S. Koh, C. H. Gan, W. K. Phua, Y. A. Akimov and P. Bai, *IEEE J. Sel. Top. Quantum Electron.*, 2014, **20**, 36–42.
42 G. Jo, S.-I. Na, S.-H. Oh, S. Lee, T.-S. Kim, G. Wang, M. Choe, W. Park, J. Yoon, D.-Y. Kim, Y. H. Kahng and T. Lee, *Appl. Phys. Lett.*, 2010, **97**, 213301.

43 S.-S. Li, K.-H. Tu, C.-C. Lin, C.-W. Chen and M. Chhowalla, *ACS Nano*, 2010, **4**, 3169–3174.
44 J. Nicasio-Collazo, J.-L. Maldonado, J. Salinas-Cruz, D. Barreiro-Argüelles, I. Caballero-Quintana, C. Vázquez-Espinosa and D. Romero-Borja, *Opt. Mater.*, 2019, **98**, 109434.
45 B.-Y. Wang, E.-S. Lee, Y.-J. Oh and H. W. Kang, *RSC Adv.*, 2017, **7**, 52914–52922.
46 A. K. Sarker and J.-D. Hong, *Langmuir*, 2012, **28**, 12637–12646.
47 N. I. Kovtyukhova, P. J. Ollivier, B. R. Martin, T. E. Mallouk, S. A. Chizhik, E. V. Buzaneva and A. D. Gorchinskiy, *Chem. Mater.*, 1999, **11**, 771–778.
48 W. S. Hummers and R. E. Offeman, *J. Am. Chem. Soc.*, 1958, **80**, 1339.
49 K. Krishnamoorthy, M. Veerapandian, K. Yun and S. J. Kim, *Carbon*, 2013, **53**, 38–49.
50 J. Liu, M. Durstock and L. Dai, *Energy Environ. Sci.*, 2014, **7**, 1297–1306.
51 M. Elshafie, M. G. Taha, S. M. Elhamamsy, Y. Moustafa and W. I. M. Elazab, *Egypt. J. Pet.*, 2020, **29**, 195–201.
52 B. Y. Chang, N. M. Huang, M. N. An'amt, A. R. Marlinda, Y. Norazriena, M. R. Muhamad, I. Harrison, H. N. Lim and C. H. Chia, *Int. J. Nanomed.*, 2012, **7**, 3379–3387.
53 E. Aliyev, V. Filiz, M. M. Khan, Y. J. Lee, C. Abetz and V. Abetz, *Nanomaterials*, 2019, **9**, 1180.
54 A. Najjar, S. Sabri, R. Al-Gaashani, V. Kochkodan and M. A. Atieh, *Appl. Sci.*, 2019, **9**, 513.
55 N. Sharma, V. Sharma, Y. Jain, M. Kumari, R. Gupta, S. K. Sharma and K. Sachdev, *Macromol. Symp.*, 2017, **376**, 1700006.
56 B. Gurzęda, P. Florczak, M. Wiesner, M. Kempiński, S. Jurga and P. Krawczyk, *RSC Adv.*, 2016, **6**, 63058–63063.
57 B. D. Ossonon and D. Bélanger, *RSC Adv.*, 2017, **7**, 27224–27234.
58 Y. Si and E. T. Samulski, *Nano Lett.*, 2008, **8**, 1679–1682.
59 K. N. Kudin, B. Ozbas, H. C. Schniepp, R. K. Prud'homme, I. A. Aksay and R. Car, *Nano Lett.*, 2008, **8**, 36–41.
60 S. Perumbilavil, P. Sankar, T. P. Rose and R. Philip, *Appl. Phys. Lett.*, 2015, **107**, 051104.
61 F. T. Johra, J.-W. Lee and W.-G. Jung, *J. Ind. Eng. Chem.*, 2014, **20**, 2883–2887.
62 R. Steim, F. R. Kogler and C. J. Brabec, *J. Mater. Chem.*, 2010, **20**, 2499–2512.
63 B. A. Chambers, M. Notarianni, J. Liu, N. Motta and G. G. Andersson, *Appl. Surf. Sci.*, 2015, **356**, 719–725.
64 V. D. Mihailetchi, J. Wildeman and P. W. M. Blom, *Phys. Rev. Lett.*, 2005, **94**, 126602.
65 W. E. I. Sha, X. Li and W. C. H. Choy, *Sci. Rep.*, 2014, **4**, 6236.
66 J. D. Morris, T. L. Atallah, C. J. Lombardo, H. Park, A. Dodabalapur and X.-Y. Zhu, *Appl. Phys. Lett.*, 2013, **102**, 033301.
67 A. Guerrero, N. F. Montcada, J. Ajuria, I. Etxebarria, R. Pacios, G. Garcia-Belmonte and E. Palomares, *J. Mater. Chem. A*, 2013, **1**, 12345–12354.
68 M. Ramar, C. K. Suman, R. Manimozhi, R. Ahamad and R. Srivastava, *RSC Adv.*, 2014, **4**, 32651–32657.
69 R. Sharma, H. Lee, V. Gupta, H. Kim, M. Kumar, C. Sharma, S. Chand, S. Yoo and D. Gupta, *Org. Electron.*, 2016, **34**, 111–117.
70 M.-J. Jin, J. Jo and J.-W. Yoo, *Org. Electron.*, 2015, **19**, 83–91.
71 B. Arredondo, B. Romero, G. Del Pozo, M. Sessler, C. Veit and U. Würfel, *Sol. Energy Mater. Sol. Cells*, 2014, **128**, 351–356.
72 E.-P. Yao, C.-C. Chen, J. Gao, Y. Liu, Q. Chen, M. Cai, W.-C. Hsu, Z. Hong, G. Li and Y. Yang, *Sol. Energy Mater. Sol. Cells*, 2014, **130**, 20–26.
73 H. S. Dehsari, E. K. Shalamzari, J. N. Gavgani, F. A. Taromi and S. Ghanbary, *RSC Adv.*, 2014, **4**, 55067–55076.
74 Y. Yang, H. Deng and Q. Fu, *Mater. Chem. Front.*, 2020, **4**, 3130–3152.